



# Spatial resolution of transport parameters in a subtropical karst conduit system during dry and wet seasons

Anna Ender<sup>1</sup> · Nadine Goepfert<sup>1</sup> · Nico Goldscheider<sup>1</sup>

Received: 21 July 2017 / Accepted: 16 February 2018 / Published online: 2 April 2018  
© Springer-Verlag GmbH Germany, part of Springer Nature 2018

## Abstract

Karst aquifers are characterized by a high degree of hydrologic variability and spatial heterogeneity of transport parameters. Tracer tests allow the quantification of these parameters, but conventional point-to-point experiments fail to capture spatiotemporal variations of flow and transport. The goal of this study was to elucidate the spatial distribution of transport parameters in a karst conduit system at different flow conditions. Therefore, six tracer tests were conducted in an active and accessible cave system in Vietnam during dry and wet seasons. Injections and monitoring were done at five sites along the flow system: a swallow hole, two sites inside the cave, and two springs draining the system. Breakthrough curves (BTCs) were modeled with CXTFIT software using the one-dimensional advection-dispersion model and the two-region nonequilibrium model. In order to obtain transport parameters in the individual sections of the system, a multi-pulse injection approach was used, which was realized by using the BTCs from one section as input functions for the next section. Major findings include: (1) In the entire system, mean flow velocities increase from 183 to 1,043 m/h with increasing discharge, while (2) the proportion of immobile fluid regions decrease; (3) the lowest dispersivity was found at intermediate discharge; (4) in the individual cave sections, flow velocities decrease along the flow direction, related to decreasing gradients, while (5) dispersivity is highest in the middle section of the cave. The obtained results provide a valuable basis for the development of an adapted water management strategy for a projected water-supply system.

**Keywords** Tracer tests · Analytical models · Spatiotemporal variations · Karst · Vietnam

## Introduction

Karst aquifers are important for the freshwater supply in many regions of the world, with roughly 20–25% of the world's population largely or entirely dependent on karst groundwater (Ford and Williams 2007). In Southeast Asia, around

215,000 km<sup>2</sup> or 10% of the mainland is covered by karst areas (Mouret 2004) and, therefore, karst aquifers constitute an important freshwater resource. In particular, they are characterized by anisotropy and heterogeneity (Stevanovic 2015), exacerbating the investigation of the water resources and, hence, the development of adapted and sustainable karst water management strategies. High flow velocities under partly turbulent flow conditions within the conduit network lead to a rapid transport of contaminants and, therefore, render the groundwater highly vulnerable to contamination. In Northern Vietnam, strong precipitation events during the rainy season intensify this problem, but extended dry seasons also pose a challenge to deal with. To ensure a continuous freshwater supply and a sustainable use of these valuable water resources, a profound understanding of these systems is crucial.

Artificial tracer tests are valuable tools to study the nature of karst systems because they can deliver clear information about hydraulic connections, spring catchment areas, transit time distributions and linear flow velocities (Atkinson et al. 1973; Brown et al. 1969; Goldscheider et al. 2008). Furthermore,

---

**Electronic supplementary material** The online version of this article (<https://doi.org/10.1007/s10040-018-1746-x>) contains supplementary material, which is available to authorized users.

---

✉ Anna Ender  
anna.ender@kit.edu

Nadine Goepfert  
nadine.goepfert@kit.edu

Nico Goldscheider  
nico.goldscheider@kit.edu

<sup>1</sup> Karlsruhe Institute of Technology, Institute of Applied Geosciences, Division of Hydrogeology, Kaiserstr. 12, 76131 Karlsruhe, Germany

relevant transport parameters can be determined by the quantitative analysis and modeling of breakthrough curves (Barberá et al. 2017; Hauns et al. 2001; Morales et al. 2007).

Tracer tests in active cave systems can be used to investigate transport mechanisms and to reveal the influence of cave structures or conduit configurations on parameters such as mean flow velocity and dispersion. However, few tracer experiments have been performed in active caves where both injection points and sampling points were within the cave system, to obtain more detailed information about internal structures—for example, Lauber et al. (2014) studied an active karst conduit network, and obtained spatially and temporally resolved information on conduit flow in the Blue Spring system (Blaubeuren, Germany). The flow velocities between the sampling points could be determined by using peak transit times, but dispersion coefficients were only calculated between the injection point and the sampling points. Recently, Dewaide et al. (2016) presented modeling results of tracer tests in the cave system of Han-sur-Lesse in South Belgium, whereby they obtained a spatial discretization of transport parameters by using the OTIS model (Runkel 1998; Runkel and Broshears 1991). This model is based on a two-region nonequilibrium (2RNE) approach to consider mobile and immobile flow regions and the influence of transient storage on the observed breakthrough curves. They assumed that the recovery rate amounts to 100% at each sampling site and that no bypaths, lateral inflows, or outflows occur; however, caves are known to be very dynamic and, in most cases, this assumption leads to oversimplification of the system. There remains a gap in knowledge regarding the spatial resolution of transport parameters for systems with bypaths, lateral inflows and outflows.

To improve the understanding of spatial variations of flow and transport parameters within a karst conduit system, tracer tests were conducted in a cave system in Northern Vietnam. At this study site, there is one main stream, entering and flowing through the cave system; however, bypaths, lateral inflows and outflows cannot be excluded. Therefore, the following four major research questions were examined: (1) what are the flow and transport characteristics of the cave system? (2) how are flow velocities and transport parameters spatially distributed within the individual sections in the vadose and phreatic zone? (3) what is the influence of flow conditions (rainy and dry seasons) on these parameters? and (4) is a multiple pulse injection approach feasible to obtain spatial discretization?

## Materials and methods

### Study site

The study area is located in the northernmost district of Vietnam, called Dong Van, with the identically named capital city (Fig. 1). It is one of the poorest and most remote areas of the

country and lies at the northern rim of the Dong Van Karst Plateau. This site was designated as a UNESCO Global Geopark in 2010, leading to the attraction of an increasing number of tourists. Massive limestone formations, mainly of Carboniferous and Permian ages, form an impressive karst landscape. The so-called Bac Son Formation (Fig. 1) has undergone several phases of regional tectonic deformation (Tran et al. 2013) and is characterized by dissected topography due to peak cluster, intra-mountain blind depressions, deep river valleys and steep slopes (Tam and Batelaan 2011). The Dong Van District and the neighboring Meo Vac District are facing increasing problems in terms of water supply and water quality.

With the extended dry seasons, groundwater recharge is mainly limited to 4–5 months in the summer (Van Nguyen et al. 2013). For the period 2000–2012, the mean annual precipitation in Dong Van amounts to 1,335 mm/year with the highest rainfall in June (285 mm) and lowest in February—(17 mm, data provided by National Center of Water Resources Planning and Investigation (NAWAPI), climate station Dong Van District, operated by Vietnam National Centre for Hydro-Meteorological Forecasting, (NCHMF)). Due to the high infiltration rates of the strongly karstified limestone, surface-water resources are scarce. Additionally, great depth to the water table in deep cave systems prohibits access to groundwater for the population (Van Nguyen et al. 2013). Northwest of Dong Van lies the Ma Le Valley (Fig. 1), located in the non-karstified Devonian units of the Mia Le Formation, which are composed of schists interbedded with sandstone, siltstone, calcareous shales and limestone lenses. The surface stream sinks into a cave system at the boundary to the Carboniferous-Permian Bac Son Formation. Large sections of the cave system were explored and mapped by the Belgian caving club SPEKUL, but there are phreatic zones in between that are not accessible without cave diving. The hydraulic gradient of the three cave sections Ma Le 1–3 (ML 1–3) decrease along the flow direction from 11% (ML 1) over 5% (ML 2) to 2% (ML 3) (D. Lagrou, SPEKUL, unpublished report, 2005; and D. Lagrou, SPEKUL, personal communication, 2017). The caves have separate entrance chambers facilitating access (Fig. 1b,c). Within approximately 1 km linear distance from the sinking stream, there are two springs, Ma Le 4 (ML 4) and Seo Ho 1 (SH 1), forming the Seo Ho River that flows into the receiving stream, the Nho Que River. The two separate cave entrances (ML 2 and ML 3) enable in-cave tracer tests and allow for a finer spatial resolution of parameters. It is planned to use the water from this cave system for the water supply of the small mountainous villages and Dong Van City. For the development of an adapted karst-water-management strategy, a hydrogeological understanding of the system is essential, including parameters such as the variability of discharge, flow and transport parameters, in addition to the chemical composition of groundwater and surface water, water quality and suspended load (Ender et al. 2017).

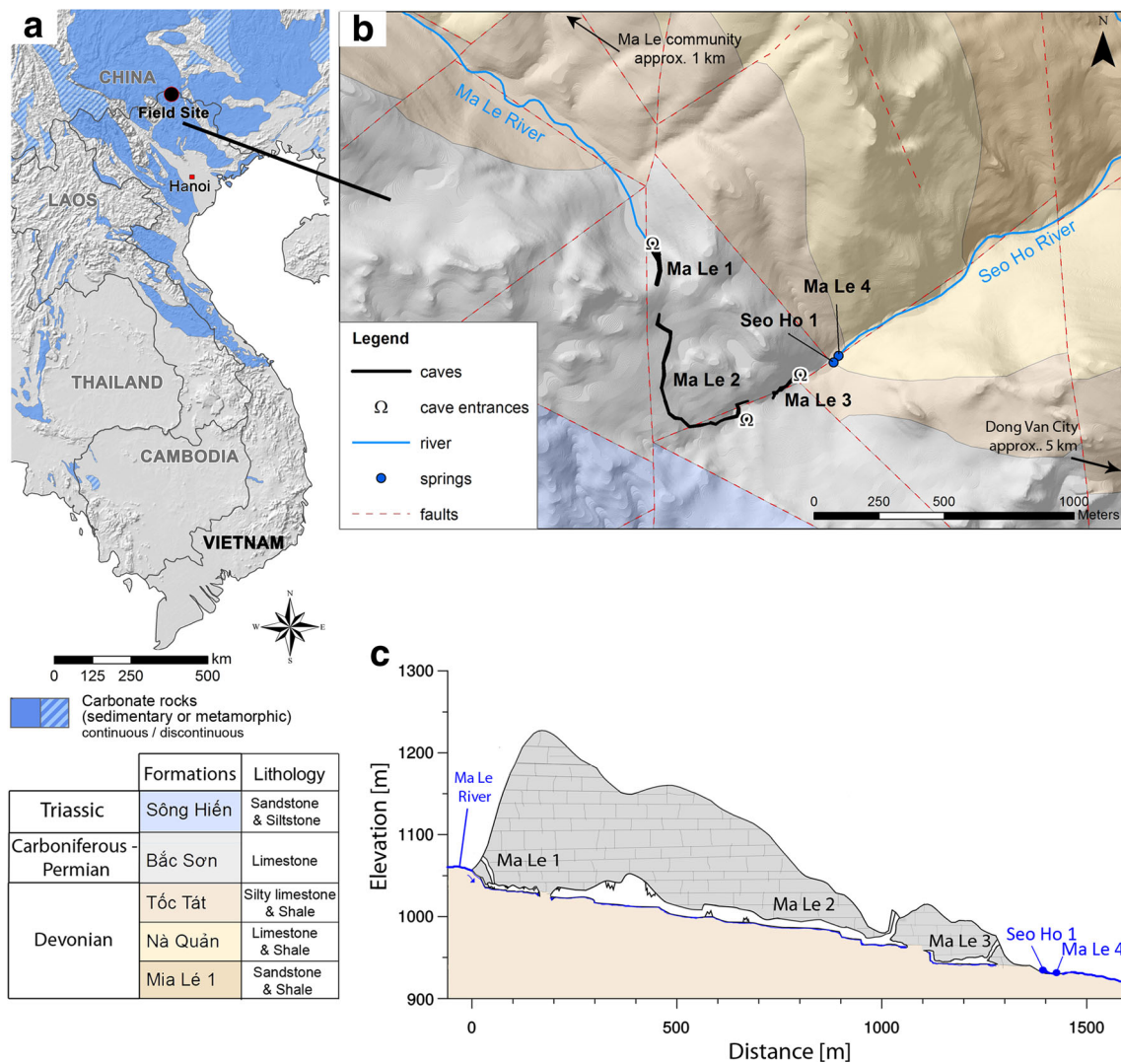


**Fig. 1** a Study area in Northern Vietnam near the Chinese border. The overview map is a section of the world karst aquifer map that exhibits the distribution of carbonate rocks (blue) in Vietnam (Chen et al. 2017). b The Ma Le cave system (D Lagrou, SPEKUL, unpublished report, 2005), shown on the 1:50,000 geological map (Vietnam Institute of Geosciences

and Mineral Resources, unpublished data, 2017) with a digital elevation model in the background (B. Zindler, A. Degen, H. Stolpe, RUB Bochum, unpublished data, 2015). c Cross section, following the course of the caves. The course of the caves is not to scale, but is, however, in the range of measured dimensions

**Tracer tests**

In total, six tracer tests (Table 1 and Fig. S1 of the electronic supplementary material (ESM)) were performed in this cave system to investigate the influences of rainy and dry seasons on flow and transport parameters and to study the structure of the cave system. Four tracer tests were conducted with an injection mass of 50 g uranine (Fluorescein Sodium, CAS: 518–47-8) into the sinking stream of the Ma Le Valley (Injection point (IP) ML 1 in Fig. S1 of the ESM). One tracer test was conducted during the dry season on 25 February 2014 (test No. 1), when discharge at ML 4 was low (72 L/s). During the rainy season, two tracer tests were performed, on 28 July 2014 and on 3 October 2015 (test Nos. 4 and 2, respectively), where the sampling points coincided with those of the test during the

dry season. The fourth tracer test, with IP ML 1 as the injection point, was performed to gain more information about flow and transport parameters under high flow conditions (16 August 2014, test No. 6), where samples were only taken at ML 4.

To investigate individual cave sections, one tracer test was conducted with a tracer injection in ML 3 (26 September 2015, test No. 5) and another one with an injection in ML 2 (29 September 2015, test No. 3). Discharge measurements were made on the day of the tracer test via the salt dilution method. The accuracy of this method is within maximum ±10% (Richardson et al. 2017), since it is constrained by the requirement of a complete mixture of salt throughout the traced stream. However, in the authors’ experience, uncertainties of the salt dilution method are usually in a range of ±2%. Nevertheless, for the calculation of uncertainties of recovery rates, a ±10%

**Table 1** Tracer tests conducted in the Ma Le cave system

No.	Date	Season	Injection point	Injection mass of uranine [g]	Sampling points	Spring discharge [L/s]
1	25.02.2014	Dry	ML 1	50	ML 2, ML 3, ML 4, SH 1	72
2	03.10.2015	Wet	ML 1	50	ML 2, ML 3, ML 4, SH 1	664
3	29.09.2015	Wet	ML 2	10	ML 3, ML 4, SH 1	690
4	28.07.2014	Wet	ML 1	50	ML 2, ML 3, ML 4, SH 1	785
5	26.09.2015	Wet	ML 3	5	ML 4, SH 1	856
6	16.08.2014	Wet	ML 1	50	ML 4	1,296

Note: Spring discharge is the discharge of *ML 4*

uncertainty of discharge rates was applied (Tables 3 and 4). Discharge rates were assumed to be constant due to the short duration of tracer tests (less than 12 h) during the rainy season. During the dry season, the discharge generally does not exhibit strong fluctuations, except after precipitation events; therefore, throughout the duration of the tracer tests (55 h), discharge can be assumed as constant.

In general, samples from the tracer tests were transported to Germany and analyzed in the laboratory using the spectrofluorometer LS55 from Perkin Elmer following standard procedures (Käss 2004). Samples from August 2014 were analyzed in Dong Van using the portable laboratory fluorometer (Trilogy, Turner Design). A field fluorometer GGUN-FL30 (Schnegg 2002) was installed in ML 3 on the 3rd of October 2015. All three fluorometers were calibrated using water from the ML 4 sampling point. The time intervals for sampling were smaller during the rainy season (1–10 min) than during the dry season (15–30 min) and were adjusted to 30 and 60 min after the main breakthrough. From the BTCs three different flow velocities can be obtained (Table 2). The mean flow velocity cannot be directly extracted from the BTC, but it is calculated by using an analytical model.

## Modeling of the results

The transport of conservative tracers can be described by the one-dimensional (1D) advection-dispersion equation (Bear 1979) as follows:

$$\frac{\partial C}{\partial t} = D \frac{\partial^2 C}{\partial x^2} - v_m \frac{\partial C}{\partial x} \quad (1)$$

**Table 2** Different flow velocities that can be yielded by tracer tests (Käss 2004)

Flow velocity	Time	Concentration
Maximum flow velocity $v_{\max}$	First detection time $t_1$	Detection limit
Peak flow velocity $v_p$	Time of peak concentration $t_p$	Maximal concentration $c_{\max}$
Mean flow velocity $v_m$	Mean residence time $t_m$	NA

NA not applicable

with  $C$  = concentration,  $t$  = time,  $D$  = longitudinal dispersion coefficient,  $x$  = distance along flow direction, and  $v_m$  = mean flow velocity.

For the analytical modeling of the observed breakthrough curves (BTCs), the software CXTFIT (Toride et al. 1999) was used. Two 1D analytical models were applied: the conventional advection-dispersion model (ADM), and the two-region nonequilibrium model (2RNE). The simplification by using a 1D model can be justified, since flow through a karst conduit can be ascribed as a 1D process and thus advection is also 1D (Goeppert and Goldscheider 2008). Some BTCs from tracer tests in karst aquifers show a distinct tailing due to immobile fluid regions, which cannot be reproduced by the ADM. The 2RNE model was developed to describe the solute exchange between mobile and immobile fluid regions as first-order mass transfer process (Toride et al. 1993). For simplification, only the dimensionless form is given (modified after Field and Pinsky 2000 and Toride et al. 1993):

$$\beta \frac{\partial C_1}{\partial T} = \frac{1}{\text{Pe}} \frac{\partial^2 C_1}{\partial Z^2} - \frac{\partial C_1}{\partial Z} - \omega(C_1 - C_2) \quad (2)$$

$$(1 - \beta) \frac{\partial C_2}{\partial T} = \omega(C_1 - C_2) \quad (3)$$

Equations (2) and (3) include additional parameters with subscripts referring to mobile (1) or immobile (2) fluid regions.  $C$  represents the dimensionless solute concentration and  $T$  and  $Z$  dimensionless time and space variables, respectively. The Peclet number,  $\text{Pe}$ , is defined by the model parameters mean flow velocity ( $v_m$ ) and dispersion coefficient ( $D$ ):

$$Pe = \frac{xv_m}{D} = \frac{x}{\alpha} \quad (4)$$

where  $x$  is the flow distance and  $\alpha$  the dispersivity. The dimensionless partitioning coefficient  $\beta$  ( $0 \leq \beta \leq 1$ ) indicates the proportion of mobile water, while the mass transfer coefficient  $\omega$  ( $> 0$ ) describes the exchange rate between the fluid regions. This model was successfully applied to the simulation of BTCs from tracer tests in karst systems (Barberá et al. 2017; Birk et al. 2005; Field and Pinsky 2000; Geyer et al. 2007; Goepfert and Goldscheider 2008; Lauber et al. 2014).

The fitting procedure is based on a nonlinear least square method (Tang et al. 2010; Toride et al. 1999; van Genuchten et al. 2012). The ADM considers two fitting parameters, advection (expressed as mean flow velocity  $v_m$ ) and dispersion (expressed as longitudinal dispersion coefficient  $D$ ), while the 2RNE includes additionally  $\beta$  and  $\omega$ . For both models, ADM and 2RNE, tracer mass was included in the fitting procedure. All parameters were calculated with real flow distances, since the course of the cave stream is essentially known. The distance for the phreatic zones between the single cave sections and for the section ML 3–ML 4, where no cave plans are available, were assumed to be linear.

Two different input scenarios were used:

1. Pulse injection (Dirac input of tracer)
2. Multi pulses injection (MPI = multiple pulse input)

The Dirac input was used to investigate flow and transport parameters from the injection point, in this case at the stream sink (IP ML 1 in Fig. S1 of the [ESM](#)), to the individual sampling point. In contrast, the MPI approach was applied to gain more information about specific cave segments between the sampling points. The input function is realized by a series of successive applications of constant solute pulses (Toride et al. 1995), which correspond to the BTCs observed inside the cave system. This enables an investigation of transport parameters between ML 2 and ML 3, for instance, without a real tracer injection in ML 2. The flow chart (Fig. 2) exhibits the straight forward procedure of the MPI approach by using the example of the section ML 3–ML 4.

The starting time of the multiple pulse injection ( $t_0$ ) corresponds to the first detection time of the BTC ( $t_1$ ), which is used as the input function. While this pragmatic procedure delivers robust model parameters by using the ADM, it does not work for the 2RNE, which results in high uncertainties. Therefore, the MPI approach was modified by using the 2RNE-modeled concentrations of the input functions. Although, there are some deviations within the modeled and observed input BTCs, this procedure delivers a good approximation of the transport parameters without such high uncertainties. With the 2RNE model, at least four different parameters were fitted at the same time, so the results are less robust

than those from the ADM (Goepfert and Goldscheider 2008; Lauber et al. 2014; van Genuchten et al. 2012). Therefore, concerning the MPI approach, the figures focus on the results obtained by the ADM; however, the results from 2RNE are additionally shown in the tables and are discussed.

For the quality evaluation of the modeling results, the coefficient of determination ( $R^2$ ), the root mean square error (RMSE) as well as a modified Nash-Sutcliffe efficiency ( $E_{j=1}$ ) were computed for each BTC simulation. The calculation of  $E_{j=1}$ , based on Luhmann et al. (2012), delivers values between 1.0 (perfect fit) and  $-\infty$ .

## Results

### Variability of flow parameters

In total, four BTCs were obtained for the main outlet of the cave system, ML 4, as shown in Fig. 3. During high flow conditions ( $Q = 1,296$  L/s), the first tracer detection took place within 1 h, resulting in a maximum flow velocity of 1,492 m/h. With the exception of the BTC on 3 October 2015, all BTC showed similar maximum tracer concentrations. The discharge ranged between 72 and 1,296 L/s, illustrating the high variability of this system.

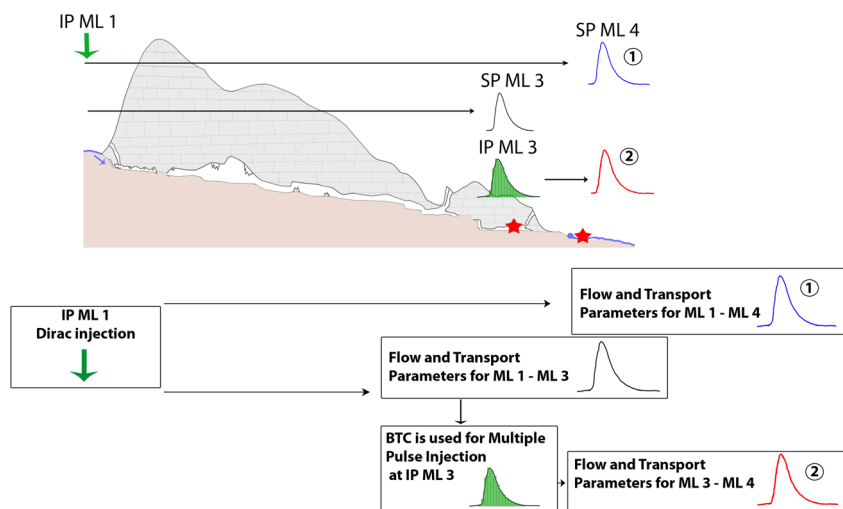
Consequently, flow and transport parameters are affected by the variation in discharge (Fig. 4). By applying an ADM, mean flow velocities for the complete cave section (ML 1–ML 4, distance 1,492 m) were between 183 m/h during the dry season (25 February 2014) and 1,043 m/h during the rainy season (16 August 2014). With increasing discharge, an increasing recovery rate was observed between 36% ( $Q = 72$  L/s) and 98% ( $Q = 1296$  L/s, Tables 3 and 4).

Dispersivity first decreased from 19 to 10 m with increasing discharge, but increased again to 21 m for higher discharge rates. The conditions of the tracer test on 28 July 2014 (785 L/s) and 3 October 2015 (664 L/s) were quite similar, leading to similar mean flow velocities (724 m/h and 663 m/h) and dispersivities (10 and 12 m). Yet, the maximum concentration on 3 October (26.65  $\mu\text{g/L}$ ) exceeded the one on 28 July (19.33  $\mu\text{g/L}$ ).

The 2RNE delivered slightly lower values for mean flow velocities and dispersivities, but the behavior with increasing discharge is similar to the ADM. Additionally, the 2RNE revealed an increase of the partition coefficient  $\beta$  from 0.81 to 0.99 with increasing discharge. The mass transfer coefficient  $\omega$  first increased and decreased again with increasing discharge, but exhibited high uncertainties.

The BTCs of ML 4 (Fig. 3) and the flow and transport parameters (Fig. 4) exhibit strong seasonal variability. To investigate the differences in flow and transport parameters in more detail, the BTCs of each sampling site within the cave system are shown in Fig. 5 for both dry and wet season.

**Fig. 2** Flow chart illustrating the procedure of the multiple pulse injection application, exemplified with the section ML 3–ML 4 and marked with the circled numbers 1 and 2. Cross section follows the course of the caves (Fig. 1b)



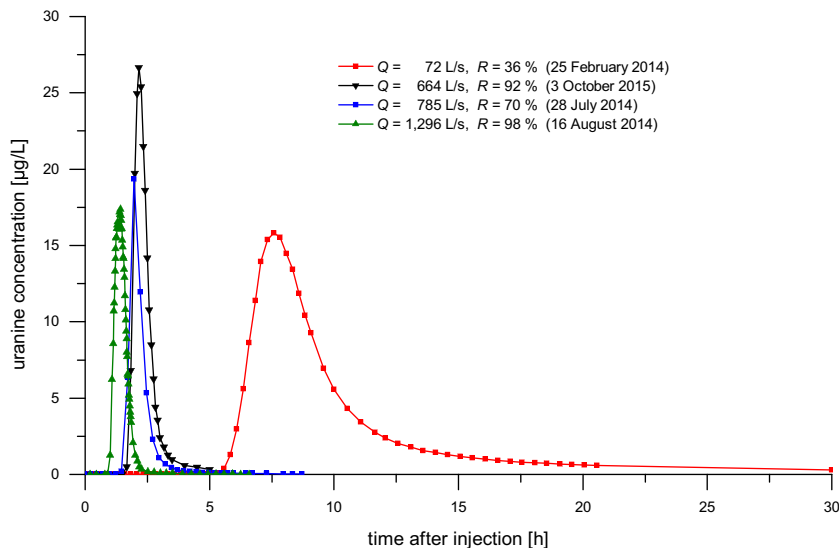
The BTCs for the second tracer test during the rainy season (28 July 2014) are exhibited in Fig. S2 of the [ESM](#). Tables 3 and 4 list all parameters for the ADM and 2RNE with the corresponding uncertainties. The following results can be summarized:

- During the rainy season, the discharge at the springs (ML 4 + SH 1) increased by 78 and 24% compared to the discharge of the sinking stream at ML 1 for July 2014 and October 2015, respectively (Tables 3 and 4). Thus, there might be an inflow within the cave system, whose contribution decreases or is even absent during the dry season, while in contrast, the springs in February 2014 exhibited a slightly smaller discharge ( $Q = 106 \text{ L/s}$ ) than the sinking stream ( $Q = 120 \text{ L/s}$ ). Although, the difference was within the uncertainty range of discharge measurement, there could be water and tracer losses along the flow path.
- The tracer recovery rate at the outlet, the karst springs ML 4 and SH 1, was higher in the rainy season (74–98%)

compared to the dry season (51%). Parallel flow paths might be partly active, since recovery rate was found to be higher at the springs than in ML 2 and ML 3. These parallel flow paths might not be active during the dry season, where the recovery rate decreased with increasing flow distance.

- A tracer injection in ML 2 resulted in a complete tracer recovery at ML 3; however, slightly lower recovery rates were found at the springs (86%).
- Depending on hydrological conditions, there have to be water gains and losses along the flow path.
- Mean flow velocities were positively correlated with discharge and were found to be increased by a factor of approximately 4 during the rainy season compared to dry season.
- Dispersivity first decreased and then increased again with increasing discharge. During the dry season, dispersivity is smallest in the ML 1–ML 2 section and highest in the sections ML 1–ML 3 and ML 1–SH 1. During the rainy

**Fig. 3** Breakthrough curves observed at the spring ML 4 under different hydrologic conditions. Discharge ( $Q$ ) and recovery rate ( $R$ ) were determined for the spring ML 4



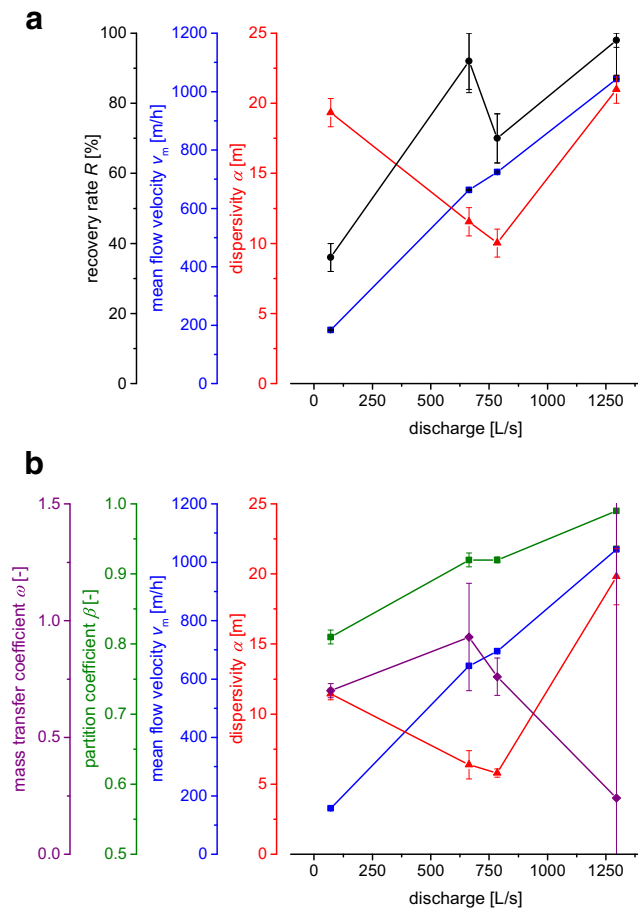


**Fig. 4** Variation of flow and transport parameters for the complete cave system (ML 1–ML 4) dependent on the spring discharge (ML 4), modeled with **a** ADM and **b** 2RNE

season, section ML 1–SH 1 exhibited the highest dispersivity, followed by the section ML 1–ML 3.

- The BTCs of the dry season showed a stronger tailing that could not be reproduced by the ADM, but rather with the 2RNE. The partition coefficient increased with increasing discharge, indicating that immobile fluid regions decreased from 19 to 1%, while during the dry season, the smallest  $\beta$  was found for section ML 1–ML 3, an increase of  $\beta$  with increasing flow path could be observed during rainy season. The mass transfer coefficient was fraught with high uncertainties. With increasing discharge,  $\omega$  first increased and decreased again. During the dry season,  $\omega$  was the smallest in the ML 1–ML 2 section, while during the rainy season, the smallest  $\omega$  was found for ML 1–SH 1.

### Spatial resolution by using the multiple pulse injection approach

In order to better understand the transport parameters of the individual cave sections, an MPI approach was applied by

using one BTC as an input function for the subsequent downstream cave section. Figure 2 illustrates the procedure of the approach used to obtain the modeled BTCs shown in Fig. 6.

Especially for the dry season, where the tailing was much more pronounced, the ADM was able to display the complete BTC when an MPI approach was applied (Fig. 6); however, concentrations were slightly overestimated, which became more obvious when examining the residuals. This resulted in an  $R^2$  of 0.985 for the ML 4 ADM (Fig. 6a, number 2), which was better than using the Dirac injection approach with an injection in ML 1 ( $R^2 = 0.964$ , Fig. 6a, number 1). The decreasing limb of the BTC was fitted by an ADM, which indicates that the tailing did not originate in the section ML 3–ML 4, but rather in ML 2–ML 3 and was, therefore, already considered within the input function. This effect was smaller for the rainy season, where the tailing was not as pronounced (MPI:  $R^2 = 0.968$  (Fig. 6b, number 2) Dirac:  $R^2 = 0.981$  (Fig. 6b, number 1)). Flow and transport parameters for all cave sections and all tracer tests are given in Tables 5 and 6.

The tailing can be fitted better with the 2RNE, resulting in significant higher  $R^2$ ,  $E_j = 1$ , and smaller RMSE. Although, dispersivity is smaller by using the 2RNE than by applying the ADM, the highest dispersivities were found for the section ML 2–ML 3. For low discharge rates, the section ML 2–ML 3 exhibited the smallest  $\beta$  (0.31), but for higher discharge rates this section had the highest values compared to the subsequent sections. While the mass transfer coefficient  $\omega$  was higher during the wet season than during the dry season, the section ML 2–ML 3 exhibited always the highest  $\omega$ . The flow and transport parameters obtained by using the ADM are illustrated in Fig. 7.

With increasing distance from the sinking stream, the mean flow velocity decreased due to a decreasing gradient in flow direction and, presumably, an increasing flow cross-sectional area. Dispersivity is highest in section ML 2–ML 3, whereas section ML 3–SH 1 displays similar values during the wet season. Regarding the segments of the cave system, dispersivity generally decreased with increasing discharge, except for segment ML 2–ML 3. Similar to the results from the complete system (ML 1–ML 4, Fig. 4), dispersivity first decreased with increasing discharge and then increased again at higher discharge rates.

## Discussion

### Variability of flow parameters

The spatial distribution of sampling points allowed for the investigation of the internal structure of the cave system. The findings of the tracer tests and the discharge measurements indicated that the Ma Le cave system is a highly dynamic system, with additional in- and outflows and partly active bypaths.

**Table 3** Flow and transport parameters for the sampling sites within the cave system and the karst springs by using a Dirac injection in ML 1, for tracer tests from February, July and August 2014

Term	Units	Dry season (25 February 2014)				Rainy season (28 July 2014)				Rainy season (16 August 2014)
		ML 1–ML 2	ML 1–ML 3	ML 1–ML 4	ML 1–SH 1	ML 1–ML 2	ML 1–ML 3	ML 1–ML 4	ML 1–SH 1	50 g uranine in ML 1 (Q ND)
<b>Injection</b>										
		50 g uranine in ML 1 (Q = 120 L/s)				50 g uranine in ML 1 (Q = 463 L/s)				50 g uranine in ML 1 (Q ND)
<b>Sections</b>										
		ML 1–ML 2	ML 1–ML 3	ML 1–ML 4	ML 1–SH 1	ML 1–ML 2	ML 1–ML 3	ML 1–ML 4	ML 1–SH 1	ML 1–ML 4
<b>Parameters</b>										
Distance	<i>x</i>	[m]	992	1,314	1,492	1,454	992	1,314	1,454	1,492
Discharge	<i>Q</i>	[L/s]	109 ± 11	128 ± 13	72 ± 7	34 ± 3	ND	ND	37 ± 4	1,296 ± 130
Tracer recovery	<i>R</i>	[%]	71 ± 7	57 ± 6	36 ± 4	15 ± 2	ND	ND	4 ± 1	98 ± 10
Maximum concentration	<i>c</i> <sub>max</sub>	[µg/L]	64.75	22.08	15.83	15.79	67.06	30.56	12.40	17.39
Peak time	<i>t</i> <sub>p</sub>	[h]	2.57	4.58	7.58	7.37	0.72	1.22	1.97	1.42
Peak velocity	<i>v</i> <sub>p</sub>	[m/h]	386	287	197	197	1,378	1,077	738	1,066
<b>ADM approach</b>										
Mean flow velocity	<i>v</i> <sub>m</sub>	[m/h]	359 ± 2	249 ± 3	183 ± 1	185 ± 2	1,350 ± 2	1,009 ± 4	650 ± 4	1,043 ± 2
Dispersion	<i>D</i>	[m <sup>2</sup> /h]	3,802 ± 292	6,653 ± 761	3,538 ± 227	4,848 ± 578	8,603 ± 272	12,240 ± 689	12,280 ± 1,366	21,900 ± 454
Dispersion	<i>α</i>	[m]	11 ± 1	27 ± 3	19 ± 1	26 ± 3	6.4 ± 0.2	12 ± 1	19 ± 2	21 ± 1
Root mean square error	RMSE	[-]	2.16	1.62	0.92	1.22	0.95	1.12	0.61	0.47
Coeff. of determination	<i>R</i> <sup>2</sup>	[-]	0.980	0.939	0.964	0.939	0.997	0.983	0.990	0.995
Nash-Sutcliffe efficiency	<i>E</i> <sub><i>j</i> = 1</sub>	[-]	0.82	0.71	0.82	0.72	0.96	0.88	0.90	0.95
<b>2RNE approach</b>										
Mean flow velocity	<i>v</i> <sub>m</sub>	[m/h]	297 ± 5	211 ± 3	157 ± 1	160 ± 3	1,332 ± 1	971 ± 4	607 ± 3	1,044 ± 6
Dispersion	<i>D</i>	[m <sup>2</sup> /h]	2,643 ± 98	2,825 ± 147	1,795 ± 56	2,102 ± 117	5,893 ± 236	6,499 ± 434	5,303 ± 1277	20,680 ± 1,727
Dispersion	<i>α</i>	[m]	9 ± 1	14 ± 1	11.4 ± 0.4	13 ± 1	4.4 ± 0.2	6.7 ± 0.5	9 ± 2	20 ± 2
Partition coeff.	<i>β</i>	[-]	0.82 ± 0.01	0.78 ± 0.01	0.81 ± 0.01	0.81 ± 0.01	0.950 ± 0.004	0.91 ± 0.01	0.909 ± 0.005	0.99 ± 0.05
Mass transfer coeff.	<i>ω</i>	[-]	0.34 ± 0.01	0.71 ± 0.04	0.70 ± 0.03	0.64 ± 0.04	0.72 ± 0.11	0.81 ± 0.11	0.43 ± 0.04	0.24 ± 2.50
Mean flow velocity (mobile prop.)	<i>v</i> <sub>m</sub> / <i>β</i>	[m/h]	362	271	194	198	1,402	1,067	667	1,055
Root mean square eError	RMSE	[-]	0.44	0.37	0.23	0.28	0.10	0.36	0.06	0.40
Coeff. of determination	<i>R</i> <sup>2</sup>	[-]	0.999	0.997	0.998	0.997	1.000	0.998	1.000	0.996
Nash-Sutcliffe efficiency	<i>E</i> <sub><i>j</i> = 1</sub>	[-]	0.97	0.94	0.96	0.94	0.99	0.96	0.98	0.95

Mean flow velocities and dispersion were obtained with the ADM and the 2RNE approach, while the partition coefficient and mass transfer coefficient were additionally yielded with the 2RNE approach. Dispersion was calculated ( $\alpha = D/v_m$ ). The standard deviation ( $\pm$  SD) for the fitted parameters was given by CXTFIT, while the uncertainty of discharge measurements was assumed to be maximal  $\pm$ 10%, based on Richardson et al. (2017). Table 4 provides further data on the parameters yielded by the tracer tests from September and October 2015. *ND* not determined; *prop.* proportion; *coeff.* coefficient



**Table 4** Flow and transport parameters for the sampling sites within the cave system and the karst springs by using a Dirac injection in ML 1, for tracer tests from September and October 2015

Injection	Term	Units	Rainy season (26 September 2015)				Rainy season (29 September 2015)				Rainy season (3 October 2015)			
			5 g uranine in ML 3 ( $Q = 849$ L/s)		10 g uranine in ML 2 ( $Q = 905$ L/s)		50 g uranine in ML 1 ( $Q = 564$ L/s)							
Sections			ML 3–ML 4	ML 3–SH 1	ML 2–ML 3	ML 2–ML 4	ML 2–SH 1	ML 1–ML 2	ML 1–ML 3	ML 1–ML 4	ML 1–SH 1			
<b>Parameters</b>														
Distance	$x$	[m]	178	140	322	500	462	992	1,314	1,492	1,454			
Discharge	$Q$	[L/s]	856 ± 86	34 ± 3	902 ± 90	690 ± 69	33 ± 3	626 ± 63	475 ± 48	664 ± 66	33 ± 3			
Tracer recovery	$R$	[%]	85 ± 9	5 ± 1	105 ± 11	82 ± 8	4 ± 1	87 ± 9	74 ± 7	92 ± 9	4 ± 1			
Maximum concentration	$c_{max}$	[µg/L]	5.27	5.39	10.28	5.82	4.16	82.04	41.46	26.65	21.81			
Peak time	$t_p$	[h]	0.60	0.72	0.5	1.15	1.33	0.75	1.37	2.17	2.22			
Peak velocity	$v_p$	[m/h]	297	194	644	435	347	1,323	959	688	655			
<b>ADM approach</b>														
Mean flow velocity	$v_m$	[m/h]	285 ± 2	181 ± 1	598 ± 5	408 ± 2	309 ± 2	1,268 ± 4	916 ± 1	663 ± 2	617 ± 4			
Dispersion	$D$	[m <sup>2</sup> /h]	645 ± 38	400 ± 28	5,106 ± 335	2,427 ± 172	2,515 ± 150	9,404 ± 451	11,700 ± 204	7,656 ± 486	7,552 ± 755			
Dispersion	$\alpha$	[m]	2.3 ± 0.2	2.2 ± 0.2	9 ± 1	6.0 ± 0.5	8 ± 1	7.4 ± 0.4	12.8 ± 0.2	12 ± 1	12 ± 1			
Root mean square error	RMSE	[-]	0.23	0.27	0.52	0.32	0.16	3.31	1.13	1.19	1.29			
Coeff. of determination	$R^2$	[-]	0.984	0.978	0.984	0.982	0.991	0.991	0.987	0.986	0.976			
Nash-Sutcliffe efficiency	$E_j = 1$	[-]	0.90	0.86	0.88	0.90	0.92	0.92	0.89	0.88	0.85			
<b>2RNE approach</b>														
Mean flow velocity	$v_m$	[m/h]	269 ± 6	175 ± 2	571 ± 4	364 ± 22	284 ± 12	1,236 ± 3	889 ± 1	645 ± 2	584 ± 10			
Dispersion	$D$	[m <sup>2</sup> /h]	434 ± 44	166 ± 49	1,531 ± 304	1,718 ± 209	1,899 ± 140	3,859 ± 1,740	5,179 ± 160	4,115 ± 453	4,104 ± 525			
Dispersion	$\alpha$	[m]	1.6 ± 0.2	1.0 ± 0.3	3 ± 1	5 ± 1	7 ± 1	3 ± 1	8.8 ± 0.2	6 ± 1	7 ± 1			
Partition coeff.	$\beta$	[-]	0.91 ± 0.02	0.86 ± 0.03	0.77 ± 0.02	0.87 ± 0.05	0.90 ± 0.03	0.86 ± 0.05	0.889 ± 0.002	0.92 ± 0.01	0.91 ± 0.01			
Mass transfer coeff.	$\omega$	[-]	0.47 ± 0.15	1.38 ± 0.63	2.12 ± 0.35	0.39 ± 0.10	0.28 ± 0.06	2.92 ± 1.43	1.36 ± 0.07	0.93 ± 0.23	0.62 ± 0.17			
Mean flow velocity (mobile prop.)	$v_m/\beta$	[m/h]	296	203	742	418	316	1,437	999	701	642			
Root mean square error	RMSE	[-]	0.16	0.17	0.19	0.24	0.10	1.42	0.32	0.41	0.66			
Coeff. of determination	$R^2$	[-]	0.993	0.992	0.998	0.991	0.997	0.998	0.999	0.998	0.995			
Nash-Sutcliffe efficiency	$E_j = 1$	[-]	0.94	0.91	0.96	0.93	0.96	0.97	0.96	0.96	0.94			

Mean flow velocities and dispersion were obtained with the ADM and the 2RNE approach, while the partition coefficient and mass transfer coefficient were additionally yielded with the 2RNE approach. Dispersion was calculated ( $\alpha = D/v_m$ ). The standard deviation ( $\pm$  SD) for the fitted parameters were given by CXTFIT, while the uncertainty of discharge measurements was assumed to be maximal  $\pm 10\%$ , based on Richardson et al. (2017). *ND* not determined; *prop.* proportion; *coeff.* coefficient

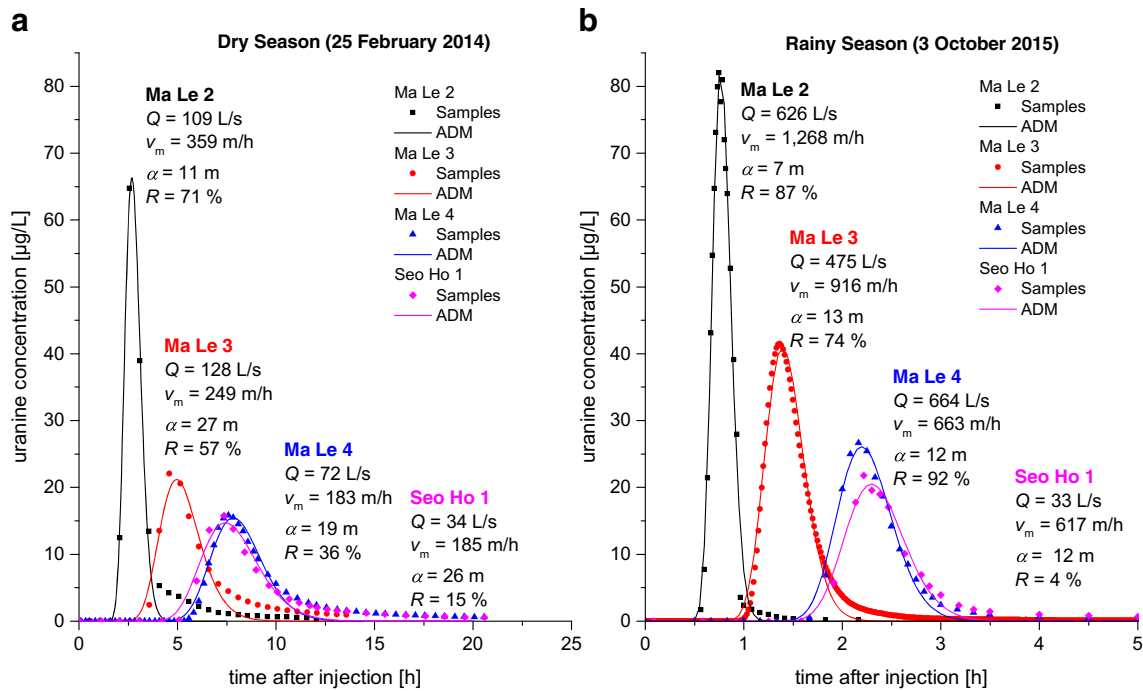


**Fig. 5** Breakthrough curves, modeled with the advection-dispersion model, for each sampling site within the cave system for both **a** dry and **b** wet season ( $Q$  discharge,  $v_m$  mean flow velocity,  $\alpha$  dispersivity,  $R$  recovery rate). The Dirac input function was applied. Note the different scales of the time axes

The total recovery rate at both springs decreased with decreasing discharge, whereby the spring SH 1 is characterized by a very constant discharge independent of flow conditions. However, recovery rates increased from 4% during the rainy

season to 15% during the dry season, since the relative contribution of SH 1 to the total discharge of both springs increased with decreasing total runoff; therefore, it is highly probable that SH 1 is fed by a conduit of limited dimensions

**Fig. 6** For ML 3, a multiple pulse injection (MPI) was applied to model the BTC in ML 4 (number 2), for **a** dry season 2014, and **b** rainy season 2014. For comparison, the ADM, modeled with a Dirac injection in ML 1, is also shown (number 1; note, numbers 1 and 2 refer to Fig. 2). In the descending branch, the MPI approach resulted in a better fitting of the tailing that is indicated by smaller residuals

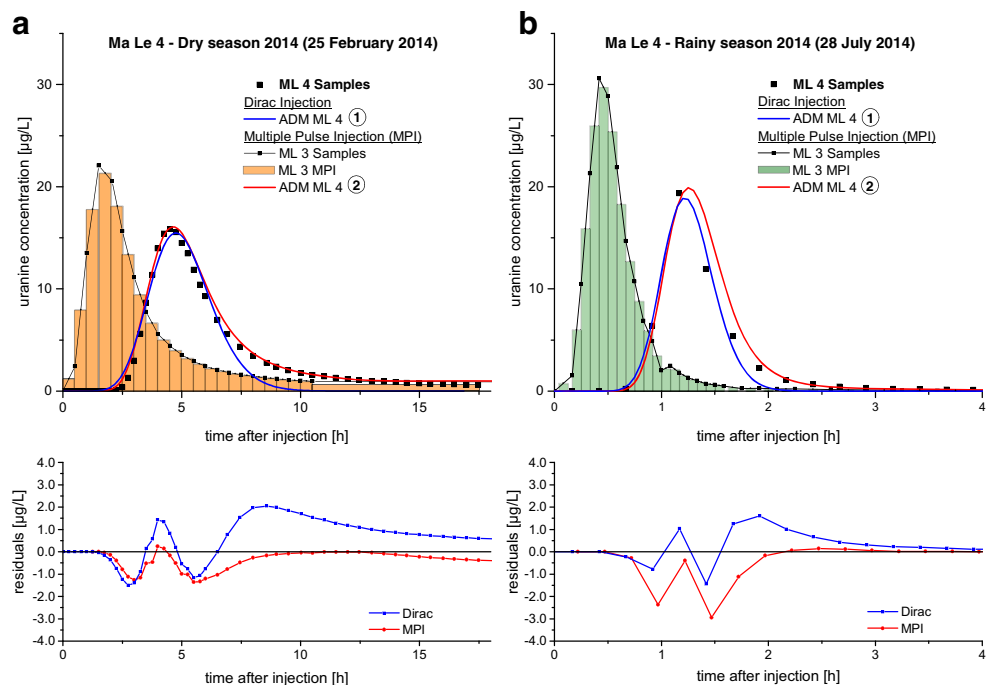


**Table 5** Flow and transport parameters for the tracer tests in *February* and *July* 2014 for the individual cave sections by using the multiple pulse injection approach and the ADM as well as the 2RNE

Term	Units	Dry season (25 February 2014)				Rainy season (28 July 2014)			
		DIRAC		MPI		DIRAC		MPI	
		ML 1–ML 2	ML 2–ML 3	ML 3–ML 4	ML 3–SH 1	ML 1–ML 2	ML 2–ML 3	ML 3–ML 4	ML 3–SH 1
Parameters									
$x$	[m]	992	322	178	140	992	322	178	140
$Q$	[L/s]	109 ± 11	128 ± 13	72 ± 7	34 ± 3	ND	ND	785 ± 79	37 ± 4
$R$	[%]	71 ± 7	57 ± 6	36 ± 4	15 ± 2	ND	ND	70 ± 7	4 ± 1
$c_{\max}$	[µg/L]	64.75	22.08	15.83	15.79	67.06	30.59	19.33	12.40
$t_p$	[h]	2.57	2.50	4.50	4.29	0.72	0.58	1.17	1.17
$v_p$	[m/h]	386	129	40	33	1378	555	152	120
ADM (observed input function)									
$v_m$	[m/h]	359 ± 2	132 ± 9	76 ± 1	74 ± 2	1,350 ± 2	621 ± 5	246 ± 4	154 ± 2
$D$	[m <sup>2</sup> /h]	3,802 ± 292	10,570 ± 1,567	690 ± 64	806 ± 110	8,603 ± 272	9,756 ± 491	1,388 ± 195	1,588 ± 144
$\alpha$	[m]	11 ± 1	80 ± 16	9 ± 1	11 ± 2	6.4 ± 0.2	16 ± 1	6 ± 1	10 ± 1
RMSE	[-]	2.16	2.12	0.64	0.58	0.95	0.87	0.80	0.30
$R^2$	[-]	0.980	0.900	0.985	0.986	0.997	0.989	0.968	0.995
$E_{j=1}$	[-]	0.82	0.72	0.89	0.90	0.96	0.89	0.84	0.91
2RNE (with 2RNE-modeled input function)									
$v_m$	[m/h]	297 ± 5	48 ± 4	44 ± 3	35 ± 4	1,332 ± 1	569 ± 5	152 ± 11	129 ± 2
$D$	[m <sup>2</sup> /h]	2,643 ± 98	1,133 ± 107	212 ± 22	194 ± 32	5,893 ± 236	4,534 ± 431	442 ± 57	678 ± 81
$\alpha$	[m]	9 ± 1	24 ± 4	5 ± 1	5 ± 1	4.4 ± 0.2	8 ± 1	3 ± 1	5 ± 1
$\beta$	[-]	0.82 ± 0.01	0.31 ± 0.02	0.61 ± 0.04	0.53 ± 0.06	0.950 ± 0.004	0.82 ± 0.01	0.58 ± 0.04	0.79 ± 0.01
$\omega$	[-]	0.34 ± 0.01	0.38 ± 0.02	0.14 ± 0.01	0.13 ± 0.01	0.72 ± 0.11	0.52 ± 0.08	0.21 ± 0.01	0.20 ± 0.02
$v_m/\beta$	[m/h]	362	155	72	66	1,402	694	262	163
RMSE	[-]	0.44	0.36	0.20	0.22	0.10	0.35	0.21	0.07
$R^2$	[-]	0.999	0.997	0.998	0.998	1.000	0.998	0.998	1.000
$E_{j=1}$	[-]	0.97	0.95	0.96	0.95	0.99	0.97	0.94	0.98

The symbols are explained in Tables 3 and 4. *ND* not determined

that diverts from the main flow path somewhere between ML 3 and ML 4. An explanation for lower recovery rates at the springs during the dry season might be another unknown (ground) spring, located in the riverbed of the Seo Ho. If the discharge capacity of the spring is limited, the relevance of this spring would increase with decreasing total discharge of the system; furthermore, the lower recovery rates during low flow conditions could be explained by retention of tracer in pools, siphons and immobile fluid regions. Part of the solute tracer was restituted from immobile to mobile fluid regions, causing a pronounced tailing (Dewaide et al. 2016).

Recovery rates, along with flow and transport parameters, exhibited a dependence on discharge, as shown in Fig. 4. Dispersivity first decreased with increasing discharge, but increased again for higher discharge rates. At small discharge rates, the cave streambed is not completely filled, so the higher dispersivity may be explained by redirections within the cave streambed and a higher relative influence of friction forces (Massei et al. 2006). With increasing discharge rates, the effect

becomes less important and the water is canalized within the conduit, leading to a smaller dispersivity. The high dispersivity at very high discharge rates could be caused by a higher water pressure to pores and fractures, a stronger interaction with conduit walls, as well as by activation of higher elevated flow paths.

The mean flow velocities appear to be smaller by using the 2RNE than by using the ADM. Since the ADM is not able to describe the tailing of the BTC, only the fast flow components are considered. In contrast, the 2RNE accounts for both the fast and slow flow components. The mean flow velocity of the mobile fluid region, obtained by dividing the mean flow velocity by  $\beta$ , was even slightly higher than yielded by the ADM (Tables 3, 4, 5 and 6). The higher dispersivity values of the ADM might be caused by immobile fluid regions that are not considered by the ADM, but that were compensated by higher dispersivity values. The difference between the dispersivity obtained by the ADM and 2RNE decreased with increasing  $\beta$  and discharge. This led to the assumption that the contribution of immobile fluid regions decreased with increasing

**Table 6** Flow and transport parameters for the tracer tests in *September* and *October* 2015 for the individual cave sections by using the multiple pulse injection approach and the ADM as well as the 2RNE

Term	Units	Rainy season (29 September 2015)			Rainy season (3 October 2015)			
		DIRAC		MPI	DIRAC		MPI	
		ML 2–ML 3	ML 3–ML 4	ML 3–SH 1	ML 1–ML 2	ML 2–ML 3	ML 3–ML 4	ML 3–SH 1
Parameters								
$x$	[m]	322	178	140	992	322	178	140
$Q$	[L/s]	902 ± 90	690 ± 69	33 ± 3	626 ± 63	475 ± 48	664 ± 66	33 ± 3
$R$	[%]	105 ± 11	82 ± 8	4 ± 1	87 ± 9	74 ± 7	92 ± 9	4 ± 1
$c_{\max}$	[µg/L]	10.28	5.82	4.26	82.04	41.46	26.65	21.82
$t_p$	[h]	0.5	0.85	1.03	0.75	0.83	1.27	1.32
$v_p$	[m/h]	644	209	136	1323	388	140	106
ADM (observed input function)								
$v_m$	[m/h]	598 ± 5	279 ± 6	154 ± 3	1,268 ± 4	525 ± 1	225 ± 6	150 ± 9
$D$	[m <sup>2</sup> /h]	5,106 ± 335	1,983 ± 260	1,079 ± 117	9,404 ± 451	7,456 ± 43	1,500 ± 291	1,852 ± 479
$\alpha$	[m]	9 ± 1	7 ± 1	7 ± 1	7.4 ± 0.4	14.2 ± 0.1	7 ± 1	12 ± 4
RMSE	[-]	0.52	0.57	0.33	3.31	0.34	2.55	3.40
$R^2$	[-]	0.984	0.939	0.962	0.991	0.995	0.931	0.825
$E_{j=1}$	[-]	0.88	0.84	0.85	0.92	0.93	0.75	0.65
2RNE (with 2RNE-modeled input function)								
$v_m$	[m/h]	571 ± 4	236 ± 13	142 ± 3	1,236 ± 3	561.4 ± 0.5	152 ± 7	70 ± 7
$D$	[m <sup>2</sup> /h]	1,531 ± 304	631 ± 133	573 ± 55	3,859 ± 1,740	2,932 ± 96	462 ± 41	161 ± 34
$\alpha$	[m]	3 ± 1	3 ± 1	4.0 ± 0.5	3 ± 1	5.2 ± 0.2	3.0 ± 0.4	2 ± 1
$\beta$	[-]	0.77 ± 0.02	0.81 ± 0.04	0.87 ± 0.02	0.86 ± 0.05	0.772 ± 0.004	0.68 ± 0.03	0.44 ± 0.04
$\omega$	[-]	2.12 ± 0.35	0.26 ± 0.08	0.23 ± 0.07	2.92 ± 1.43	1.03 ± 0.03	0.20 ± 0.01	0.42 ± 0.03
$v_m/\beta$	[m/h]	742	291	163	1,437	729	224	159
RMSE	[-]	0.19	0.26	0.09	1.42	0.15	0.34	0.61
$R^2$	[-]	0.998	0.989	0.998	0.998	0.999	0.999	0.995
$E_{j=1}$	[-]	0.96	0.92	0.96	0.97	0.96	0.97	0.94

The symbols are explained in Tables 3 and 4. *ND* not determined

discharge as already assumed by Barberá et al. (2017); although unfortunately,  $\omega$  contained high uncertainties.

### Multiple-pulse-injection approach

The MPI approach is suggested to be a valuable tool to obtain more information about the spatial variation of transport parameters within cave systems. It clearly revealed that the highest dispersivities were found in the sections ML 2–ML 3 and ML 3–SH 1, most likely controlled by the cave structure. Particularly, macrodispersivity is formation-specific and not only scale dependent, as shown by Zech et al. (2015). During the dry season, the high dispersivity in the section ML 2–ML 3 yielded by the ADM could be partly explained by pools and siphons and a larger phreatic passage, thus by a higher content of immobile fluid regions. The 2RNE supported this assumption, since the fraction of mobile water only amounted to 31%; however, during the rainy season the proportion of immobile fluid regions was smallest in this section (highest  $\beta$ ), while

dispersivity was still the highest. So, the high dispersivity values of the ADM are not only caused by the compensation of immobile fluid regions, but might be caused by slower flow components due to friction forces (Massei et al. 2006). At the same time,  $\omega$  indicated a higher exchange rate between mobile and immobile fluid regions in the section ML 2–ML 3, meaning more of the initial tracer mass in the mobile fluid region had time to equilibrate with tracer mass in the immobile fluid region (Field and Pinsky 2000). This led to the assumption that sections with small proportions of immobile fluid zones but high dispersivity show higher exchange rate between mobile and immobile fluid regions. With increasing discharge and flow velocities, the contribution of immobile fluid regions was generally reduced in the cave sections, leading to lower dispersivity values when using an ADM and higher  $\beta$  values with the 2RNE. The high dispersivity in the section ML 3–SH 1 can be explained by the smaller dimensions of this section and by the interaction with the conduit walls. This interaction likely enhances the inhomogeneity of the velocity profile and

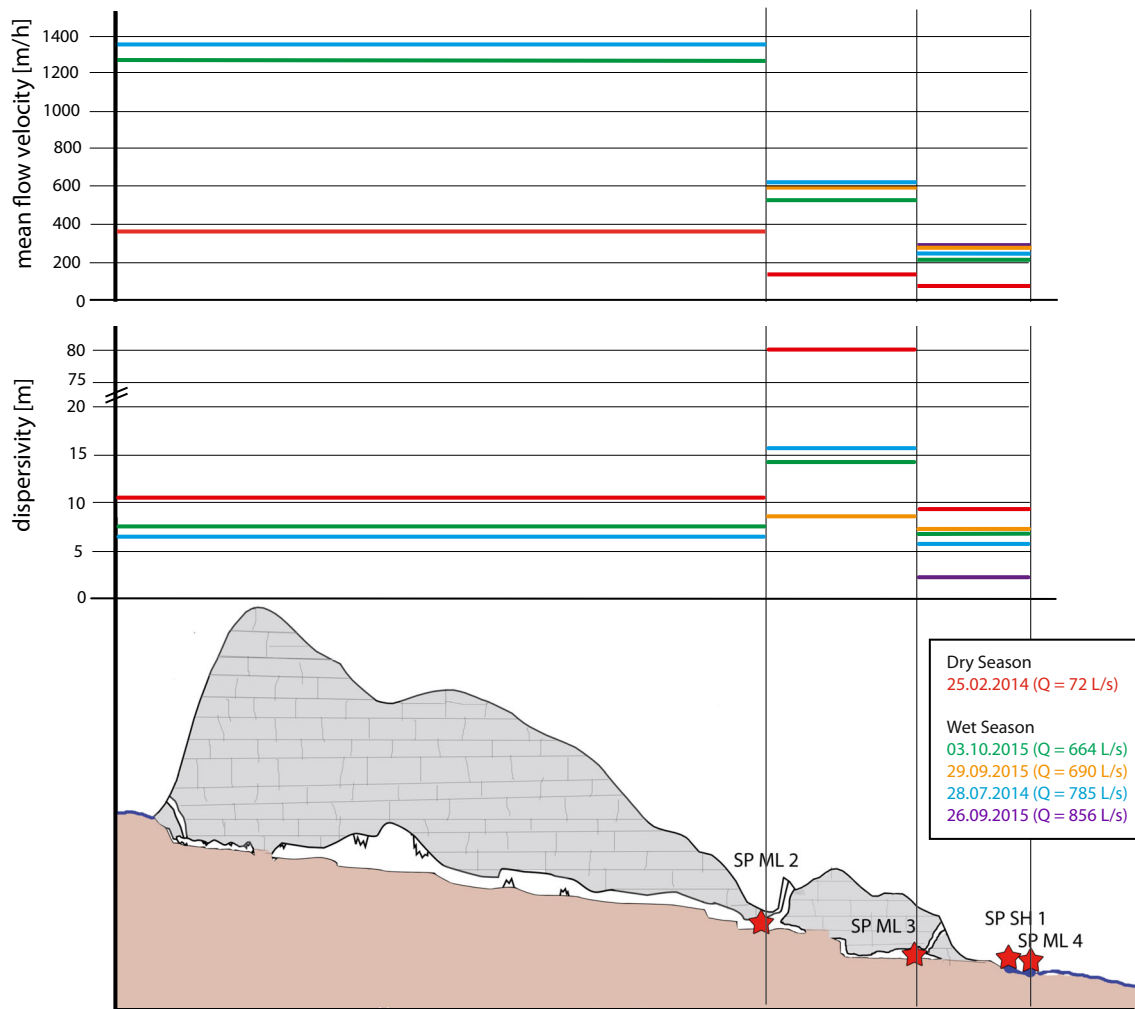


**Fig. 7** Spatial resolution of flow and transport parameters within the cave system. Mean flow velocity ( $v_m$ ) and dispersivity ( $\alpha$ ) are calculated with an ADM and a Dirac input for the first segment and a MPI input function for all subsequent segments. The parallel flow path ML 3–SH 1 is not

considered in this figure, but exhibits lower mean flow velocities and higher dispersivity than ML 3–ML 4 (Tables 5 and 6). The cross section follows the course of the caves (Fig. 1b)

leads to smaller mean flow velocities and a higher dispersion, as described in Hauns et al. (2001).

In general, the MPI approach revealed a progressive decrease of mean flow velocities along the flow path. This observation was already shown by Worthington (2009) and is also described in Lauber et al. (2014). It is caused by a decreasing gradient, which is most likely associated with an increase in the extent of phreatic zones. Within the phreatic zones, the area of flow cross-section is increased, leading to a further reduction of flow velocities.

The comparison of flow and transport parameters obtained by a Dirac and an MPI injection, as a function of discharge, supported the suitability of the approach, since the Dirac injection produced no outliers compared to the MPI values (Fig. S3 of the [ESM](#)). However, the comparison revealed that dispersivity obtained from the Dirac injection appears low compared to the values yielded by the MPI approach.

This could be explained by the identified bypaths from ML 1 and ML 2 to the springs that are partly active. The MPI approach assumes a tracer injection in ML 3, but if bypaths from ML 1 are active, an additional tracer input takes place from the real tracer injection in ML 1. Such a confluence of tributaries might increase dispersion (Hauns et al. 2001) and can lead to an apparent enhanced dispersivity for the section ML 3–ML 4 by using the MPI approach. In such a case, the yielded parameters consider the studied section, as well as the bypath, and consequently differ from a Dirac injection.

To obtain clear evidence of the applicability of the MPI approach, a combined tracer test should be performed with a Dirac injection in ML 1 for the MPI approach in ML 2 and ML 3, and simultaneous Dirac injections in ML 2 and ML 3 with different tracers. However, tracers with equal transport behavior should be used, which is challenging.

## Conclusions

Six tracer tests were performed in a cave system in Northern Vietnam to characterize flow and transport parameters under highly variable flow conditions that are influenced by extended dry and wet seasons. A multiple-pulse-injection approach enabled a spatial resolution of flow and transport parameters and led to a better understanding of the active karst system that can be concluded as followed:

- Flow and transport parameters are subject to strong variability depending on hydrological conditions. The mean flow velocity for the whole cave system (ML 1–ML 4) increased from 183 to 1,043 m/h with increasing discharge (72–1,296 L/s), whereby recovery rate increased from 36% to 98%. Dispersivity first decreased from 19 m to 10 m and increased again to 21 m with increasing discharge.
- With increasing discharge the impact of immobile fluid regions, expressed by the partition coefficient  $\beta$ , on flow and transport parameters decreased.
- The cave system consists not only of a sinking stream that enters the cave system and reemerges at the springs. Instead, the system is composed of further contributions, which vary in quantity depending on the hydrological conditions.
- There is not only one cave stream, but also smaller parallel flow paths. Such a bypath likely runs from ML 1 and ML 2 to the springs, whereby other flow paths could be activated depending on discharge rates.
- There is no indication that bypaths constrain the application of the MPI approach. However, it has to be considered that yielded transport parameters are influenced by potential bypaths.
- By using the multiple pulse input approach, a spatial resolution could be achieved not only for flow velocities, but also for transport parameters.
- While the combination of the MPI approach and the ADM delivered reliable parameters, an adjustment was necessary to combine the MPI with the 2RNE. For the injection function the concentrations, modeled with the 2RNE were used instead of the observed concentrations.
- It could be clearly shown that the sections ML 2–ML 3 and ML 3–SH 1 are characterized by the highest dispersivity, which leads to the generation of hypotheses concerning the structure of the system.

In the section ML 2–ML 3, the high dispersivity resulted from the ADM, can partly be explained by a higher proportion of immobile fluid regions due to pools, siphons and a larger extent of phreatic zones, as shown by a smaller  $\beta$ . The high dispersivity for ML 3–SH 1 might be caused by the smaller conduit dimension and the enhanced interaction with the conduit wall.

Generally, in-cave tracer tests were validated again as a powerful tool to investigate karst aquifers. The MPI approach enables a more detailed insight into the spatial resolution of transport parameters within the conduit system. This study revealed that karstic systems are highly dynamic and cannot be considered as static systems. Such high variabilities in flow and transport parameters impose a particularly big challenge for the usage of karst water resources in terms of technical requirements, but also in terms of water quality.

**Acknowledgements** We gratefully acknowledge the financial support of the German Federal Ministry of Education and Research (BMBF) [grant number 02WCL1291A]. We want to thank Ha Giang Peoples Committee, Dong Van Peoples Committee as well as the Vietnam Institute of Geosciences and Mineral Resources (Hanoi) for their support during fieldwork. Special thanks are given to the whole sampling team, especially to Arno Hartmann, Marian Bechtel, Philipp Holz, Alexandra Roth, Christian Weippert and Tobias Zaege and to the colleagues from VIGMR. Furthermore, we thank the cavers from the Belgian SPEKUL club, particularly David Lagrou, for their support during the tracer tests and the provision of cave maps and Nguyet Vu Thi Minh, for borrowing the field fluorimeter. We thank Arica Beisaw for proofreading and the associate editor, Prof. Luhmann, as well as the three anonymous reviewers for their valuable comments.

## References

- Atkinson TC, Smith DI, Lavis JJ, Witaker RJ (1973) Experiments in tracing underground waters in limestones. *J Hydrol* 19:323–349
- Barberá JA, Mudarra M, Andreo B, De la Torre B (2017) Regional-scale analysis of karst underground flow deduced from tracing experiments: examples from carbonate aquifers in Malaga province, southern Spain. *Hydrogeol J* 26(1):23–40
- Bear J (1979) *Hydraulics of groundwater*. McGraw-Hill, New York
- Birk S, Geyer T, Liedl R, Sauter M (2005) Process-based interpretation of tracer tests in carbonate aquifers. *Ground Water* 43:381–388
- Brown MC, Wigley TL, Ford DC (1969) Water budget studies in karst aquifers. *J Hydrol* 9:113–116
- Chen Z, Auler AS, Bakalowicz M, Drew D, Griger F, Hartmann J, Jiang G, Moosdorf N, Richts A, Stevanovic Z, Veni G, Goldscheider N (2017) The world Karst aquifer mapping project: concept, mapping procedure and map of Europe. *Hydrogeol J* 25:771–785. <https://doi.org/10.1007/s10040-016-1519-3>
- Dewaide L, Bonniver I, Rochez G, Hallet V (2016) Solute transport in heterogeneous karst systems: dimensioning and estimation of the transport parameters via multi-sampling tracer-tests modelling using the OTIS (one-dimensional transport with inflow and storage) program. *J Hydrol* 534:567–578. <https://doi.org/10.1016/j.jhydrol.2016.01.049>
- Ender A, Goepfert N, Grimmeisen F, Goldscheider N (2017) Evaluation of  $\beta$ -d-glucuronidase and particle-size distribution for microbiological water quality monitoring in Northern Vietnam. *Sci Total Environ* 580:996–1006. <https://doi.org/10.1016/j.scitotenv.2016.12.054>
- Field MS, Pinsky PF (2000) A two-region nonequilibrium model for solute transport in solution conduits in karstic aquifers. *J Contam Hydrol* 44:329–351
- Ford D, Williams P (2007) *Karst hydrogeology and geomorphology*. Wiley, Chichester, UK

- Geyer T, Birk S, Licha T, Liedl R, Sauter M (2007) Multitracer test approach to characterize reactive transport in karst aquifers. *Ground Water* 45:36–45
- Goepfert N, Goldscheider N (2008) Solute and colloid transport in karst conduits under low-and high-flow conditions. *Ground Water* 46:61–68
- Goldscheider N, Meiman J, Pronk M, Smart C (2008) Tracer tests in karst hydrogeology and speleology. *Int J Speleol* 37:3. <https://doi.org/10.5038/1827-806X.37.1.3>
- Hauns M, Jeannin P-Y, Atteia O (2001) Dispersion, retardation and scale effect in tracer breakthrough curves in karst conduits. *J Hydrol* 241: 177–193
- Käss W (2004) Geohydrologische Markierungstechnik [Geohydrological tracer technique]. Borntraeger, Stuttgart, Germany
- Lauber U, Ufrecht W, Goldscheider N (2014) Spatially resolved information on karst conduit flow from in-cave dye tracing. *Hydrol Earth Syst Sci* 18:435–445. <https://doi.org/10.5194/hess-18-435-2014>
- Luhmann AJ, Covington MD, Alexander SC, Chai SY, Schwartz BF, Groten JT, Alexander EC (2012) Comparing conservative and non-conservative tracers in karst and using them to estimate flow path geometry. *J Hydrol* 448:201–211
- Massei N, Wang HQ, Field MS, Dupont JP, Bakalowicz M, Rodet J (2006) Interpreting tracer breakthrough tailing in a conduit-dominated karstic aquifer. *Hydrogeol J* 14:849–858
- Morales T, de Valderrama IF, Uriarte JA, Antigüedad I, Olazar M (2007) Predicting travel times and transport characterization in karst conduits by analyzing tracer-breakthrough curves. *J Hydrol* 334:183–198
- Mouret C (2004) Asia, southeast In: Gunn J (ed) *Encyclopedia of Caves and Karst Science*. Fitzroy Dearborn, New York, pp 210–217
- Richardson M, Moore RD, Zimmermann A (2017) Variability of tracer breakthrough curves in mountain streams: implications for streamflow measurement by slug injection. *Can Water Res J* 42: 21–37
- Runkel RL (1998) One-dimensional transport with inflow and storage (OTIS): a solute transport model for streams and rivers. US Geological Survey, Reston, VA
- Runkel RL, Broshears RE (1991) One-dimensional transport with inflow and storage (OTIS): a solute transport model for small streams. CADSWES, Univ. of Colorado, Boulder, CO
- Schnegg P-A (2002) An inexpensive field fluorometer for hydrogeological tracer tests with three tracers and turbidity measurement. XXXII IAH and ALHSUD congress on Groundwater and Human Development, Mar del Plata, Argentina, Balkena, Rotterdam, The Netherlands, pp 1484–1488
- Stevanovic Z (2015) *Karst aquifers-characterization and engineering*. Springer, Cham, Switzerland
- Tam VT, Batelaan O (2011) A multi-analysis remote-sensing approach for mapping groundwater resources in the karstic Meo Vac Valley, Vietnam. *Hydrogeol J* 19(2):275–287. <https://doi.org/10.1007/s10040-010-0684-z>
- Tang G, Mayes MA, Parker JC, Jardine PM (2010) CXTFIT/excel—a modular adaptable code for parameter estimation, sensitivity analysis and uncertainty analysis for laboratory or field tracer experiments. *Comput Geosci* 36:1200–1209
- Toride N, Leij FJ, Van Genuchten MT (1993) A comprehensive set of analytical solutions for nonequilibrium solute transport with first-order decay and zero-order production. *Water Resour Res* 29: 2167–2182
- Toride N, Leij FJ, Van Genuchten MT (1995) The CXTFIT code for estimating transport parameters from laboratory or field tracer experiments. US Salinity Laboratory, Riverside, CA
- Toride N, Leij FJ, Van Genuchten MT (1999) The CXTFIT code for estimating transport parameters from laboratory or field tracer experiments. Research report no. 137 US Salinity Laboratory, Riverside, CA
- Tran HT, Van Dang B, Ngo CK, Hoang QD, Nguyen QM (2013) Structural controls on the occurrence and morphology of karstified assemblages in northeastern Vietnam: a regional perspective. *Environ Earth Sci* 70:511–520. <https://doi.org/10.1007/s12665-011-1057-1>
- van Genuchten MT, Šimůnek J, Leij FJ, Toride N, Šejna M (2012) STANMOD: model use, calibration, and validation. *Am Soc Agric Biol Eng* 55(4):1353–1366
- Van Nguyen L, Nguyen NK, Van Hoang H, Tran TQ, Vu NT (2013) Characteristics of groundwater in karstic region in northeastern Vietnam. *Environ Earth Sci* 70:501–510. <https://doi.org/10.1007/s12665-012-1548-8>
- Worthington SR (2009) Diagnostic hydrogeologic characteristics of a karst aquifer (Kentucky, USA). *Hydrogeol J* 17:1665
- Zech A, Attinger S, Cvetkovic V, Dagan G, Dietrich P, Fiori A, Rubin Y, Teutsch G (2015) Is unique scaling of aquifer macrodispersivity supported by field data? *Water Resour Res* 51:7662–7679